Lifetime prediction methodology for variable fretting fatigue loading: Plasticity effect

Camille Gandiolle, Siegfried Fouvry, Éric Charkaluk

Lifetime prediction methodology for variable fretting fatigue loading: plasticity effect

Camille Gandiolle[1*], Siegfried Fouvry[1], E. Charkaluk[2]

[1]LTDS UMR 5513, Ecole Centrale de Lyon, 36 Avenue Guy de Collongues, 69134 Ecully Cedex, France
[2]LML UMR 8107, Ecole Centrale de Lille, Cité Scientifique-CS 20048, 59651 Villeneuve d'Ascq Cedex, France
*corresponding author

E-mail addresses: camille.gandiolle@ec-lyon.fr, siegfried.fouvry@ec-lyon.fr, eric.charkaluk@ec-lille.fr

Nomenclature

a	Half-width of the contact area (mm)
b	Crack length (µm)
b_{CA}	Crack arrest length (µm)
$b_{ø}$	Short-to-long crack transition length (µm)
b_{opt}	Optimal crack initiation length (µm)
b_p	Propagation crack length (µm)
D	Crack nucleation damage
E	Young's modulus (MPa)
K	Stress Intensity Factor (SIF) (MPa.m$^{1/2}$)
	Fatigue crack driving force parameter (MPa.m$^{1/2}$)
K_e	Potential drop slope
K_I	Mode I SIF (MPa.m$^{1/2}$)
K_{IC}	Critical SIF (MPa.m$^{1/2}$)
ΔK	Nominal SIF (MPa.m$^{1/2}$)
$\Delta K_{ø}$	Long-crack SIF range threshold (MPa.m$^{1/2}$)
ΔK_{th}	Crack arrest condition (MPa.m$^{1/2}$)
$\underline{\quad}$	Amplitude of the second invariant of the stress tensor deviator
ℓ	Critical distance (µm)
$ℓ_{opt}$	Optimal critical distance (µm)
N	Number of cycles
N_{CN}	Number of cycles to crack nucleation cycles
N_P	Number of cycles to crack propagation cycles
N_T	Total number of numerical cycles $N_T=N_{CN}+N_P$
P	Normal force (N)
p_{max}	Maximum surface pressure (MPa)
Q	Tangential fretting force (N)
Q*	Linear tangential fretting force amplitude (N/mm)
Q^*_{CN}	Crack nucleation threshold (N/mm)
q_{max}	Maximum surface shear stress (MPa)
R	Cylinder radius (mm)
R_F	Fatigue stress ratio ($\sigma_{F,min}/\sigma_{F,max}$)
R_K	SIF stress ratio (K_{Imin}/K_{Imax})

R_Q	Fretting stress ratio (Q_{min}/Q_{max}=-Q*/+Q*)
S	Deviatoric part of
V	Potential
W	Fatigue sample thickness (mm)
δ	Fretting displacement (µm)
ε	Strain
ε_p	Plastic strain
$\Delta\varepsilon^p$	Plastic strain increment by cycle
μ	Coefficient of friction
σ	Stress (MPa)
σ_{11}	Stress along x direction (MPa)
σ_C	Crossland equivalent stress (MPa.$m^{1/2}$)
σ_d	Traction-compression fatigue limit (R_F=-1) (MPa)
σ_F	Fatigue stress (MPa)
$\sigma_{H,max}$	Maximum hydrostatic stress (MPa)
σ_y	Cyclic yield stress (MPa)
$\sigma_{y,0.2\%}$	Monotonic yield stress (MPa)
$\sigma_{y,flat}$	Cyclic yield stress of the flat material (MPa)
τ_d	Torsion fatigue limit (R_F=-1) (MPa)
	Stress tensor

Subscripts and abbreviations

CA	Crack Arrest
CEP	Cyclic elastic-plastic
E	Elastic
exp	Experimental
FF	Fretting Fatigue
max	Maximum value
mean	Mean value
MEP	Monotonic elastic-plastic
min	Minimum value
PD	Potential Drop
PF	Plain Fretting
th	Theoretical

Abstract

Both experimental and numerical approaches were developed to follow cracking damage in steel cylinder/plane fretting fatigue contact subjected to variable loading conditions.

For the experimental approach, the potential drop technique was implemented on the fretting fatigue test device to observe on-line crack propagation. A calibration curve relating crack length and potential provided direct knowledge of cracking status.

Numerically, total life was separated between crack nucleation and crack propagation. To formalize crack nucleation prediction, Crossland multiaxial fatigue behavior was applied at a critical distance to take into account the severe fretting fatigue gradients. The crack propagation rate was formalized using Kujawski's fatigue crack driving force parameter, $\overline{K}^*$, and coupling the Paris law of the material.

Using this combined crack-nucleation/crack-propagation analysis, constant fretting fatigue conditions and variable fretting fatigue sequences were investigated. Good correlations were observed.

Finally, the influence of different plastic laws was investigated. Both monotonic and cyclic approximations provided good correlation with experimental data, the cyclic description being closer.

Key-words: cracking; fretting fatigue; variable loading; FEM; plasticity

1 Introduction

Fretting is defined as a small-amplitude oscillatory movement between two surfaces in contact [1,2]. Fretting involves two sliding conditions depending on displacement amplitude: partial slip, which involves an inner stick zone, and larger-amplitude gross slip, inducing a full sliding response in the interface. The present study focused on the partial slip condition, which leads primarily to cracking damage [3,4].

Fretting cracking is often combined with cyclic bulk fatigue loading (Fig. 1a). Fretting fatigue loading can induce premature failure of the assembly. Fretting fatigue experiments aim to represent industrial condition, usually with variable loading. It is essential to be able to predict assembly lifetime, especially for variable loading applied for very large number of cycles, as experimental validation is often too expensive.

Numerous methods have been adopted to predict the lifetime of components subjected to fretting fatigue cracking damage. Navarro et al. [5] showed that accurate prediction of lifetime under fretting fatigue requires considering both crack initiation life and crack propagation life. Depending on the loading amplitude, one stage may supplant the other, but this depends on so many parameters that it is easier to consider both phases directly. The more recent works by Vázquez et al., Hojjati-Talemi et al. and Shen et al. [6–8] are in agreement, and estimated lifetime by decoupling the crack nucleation and crack propagation phases.

Crack nucleation life is usually investigated by applying a multiaxial fatigue criterion [9]. Predictions were improved by considering the severe stress gradients imposed by contact loading, using non-local process volume stress averaging strategy [10,11] or equivalent critical distance [12]. Recently, other techniques using the theory of continuum damage mechanics [8,13,14] have been explored to predict fretting crack nucleation life. Once a crack is nucleated, depending on the loading amplitude, it will propagate or reach a crack arrest condition. The usual method, for crack propagation, employs a fracture mechanics approach [7,15,16]. Crack arrest prediction used Araujo et al.'s [17] short crack arrest strategy; crack propagation was usually quantified using the Paris law.

The objective of this study was to assess prediction of fretting fatigue endurance under variable loading conditions by this sequential crack-nucleation/crack-propagation approach, and how prediction is affected by the choice of the plastic law used to simulate the fretting fatigue contact.

These two aspects were addressed by the following strategy. Extending a previous study [18], fretting fatigue endurance and crack-arrest conditions were investigated combining experiments and simulations on an uncoupled approach:

(1)

This fretting fatigue endurance was correlated with a crack-extension analysis so that:

$b=b_{\emptyset}\,(N=N_{CN})+b_p$ (Paris long-crack description) (2)

so that

- if $b<b_{\emptyset}\ \forall\ N_{CN}$: no crack nucleation;
- if $b\rightarrow b_{CA}$: crack arrest condition;
- if $b\rightarrow b_{failure}$: failure condition

with b crack length, $b_{ø}$ short-to-long crack transition length, b_p propagation crack length, b_{CA} crack length at crack arrest, $b_{failure}$ crack length at failure, N_{CN} the number of cycles to crack nucleation and N_P the number of cycles to crack propagation.

In this study, a conventional finite elements (FE) approach was used to establish the elastic shakedown stress-field condition.
Crack nucleation was defined using Crossland's criterion, applied at a critical distance to take into account the contact stress gradient effects. Special care was taken in defining the optimal critical distance, allowing minimum scatter in the crack nucleation prediction [18]. The crack nucleation law was calibrated from reserve analysis of plain fretting experiments, to establish optimal critical distance according to crack-nucleation life.
For crack propagation, an uncoupled approach, using a weight function to estimate the stress intensity factor, was applied. Crack propagation rate was defined using Kujawski's fatigue-crack driving-force parameter $\overline{K}^*$ and coupling the Paris law of the material. Predicted crack extensions were compared with experimental potential-drop measurements.

All this analysis was developed with a representative cyclic elastic-plastic law. To evaluate how chosen given plastic law affects fretting fatigue prediction, a similar analysis was performed using a simpler elastic-plastic law determined by monotonic tensile test and, finally, basic elastic behavior. For all these constitutive laws, the corresponding fatigue data were extracted and the respective fretting fatigue endurance predictions were compared.

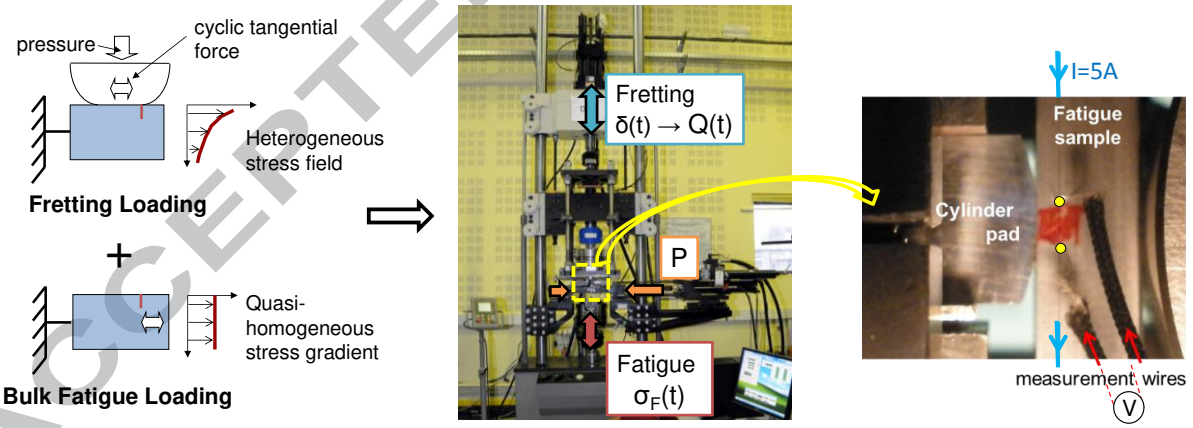

Fig. 1: (a) Illustration of the fretting fatigue loading and severe stress gradient induced; (b) photo of the fretting fatigue test set-up at the LTDS laboratory; (c) implementation of potential-drop method on the fretting fatigue sample for online crack monitoring.

2 Variable loading fretting fatigue tests

2.1 Fretting fatigue contact materials

The study material was 32Cr1 industrial steel, with low cyclic yield stress ($\sigma_{y,flat}$). Its atomic composition is given in Table 1 [19]. The material was tested under fretting fatigue conditions using a cylinder/plane contact. The cylinder was in FM35 steel of R=4.6 mm radius, applied with a normal force P on the flat material. The cylinder material was selected with higher cyclic yield stress than the flat material ($\sigma_{y,cylinder}$=1.25x$\sigma_{y,flat}$), so was less likely to nucleate a crack. Hence, cracking was investigated on the plane specimen only.

Table 1: % Atomic composition of 32Cr1 steel [19]

C	Cr	Mn	Si	Cu	Mo	Ni	Al	P	S
0.32	0.347	0.743	0.201	0.046	0.016	0.047	0.013	0.007	0.002

Normal force P was chosen high enough to generate plastic conditions in both plane and cylinder specimens, with $p_{max}=3.2\sigma_{y,flat}$ ($\sigma_{y,flat}$ being the cyclic yield stress of the flat material). Consequently, both plane and cylinder had to be described using elastic-plastic laws. For each material, tensile tests were performed to establish monotonic stress-strain behavior (Fig. 2a). Monotonic mechanical parameters E and $\sigma_{y,0.2\%}$, derived from the monotonic behavior are given in Table 2.

Table 2: Mechanical properties of cylinder and flat materials

Material	Poisson's ratio	Monotonic Parameters		Cyclic Parameters		
		E (GPa)	$\sigma_{y,0.2\%}$ (MPa)	E (GPa)	σ_y (MPa)	$p_{prager}=(\sigma-\sigma_{y,flat})/d\varepsilon_p$
Flat (32C1)	0.3	200	0.7 x$\sigma_{y,flat}$	195	$\sigma_{y,flat}$	11.7
Cylinder (FM35)	0.3	200	1.05 x$\sigma_{y,flat}$	205	1.25x$\sigma_{y,flat}$	24.8

Then, dedicated strain-controlled cyclic tests were performed to identify a cyclic elastic-plastic law. Deformation range was 0.2% to 1.5%, at a deformation rate of $5x10^{-3}s^{-1}$, with 10 cycles at each 0.1% deformation step. Fig. 2b shows stabilized stress-strain loop for 0.5% deformation in the flat material (32C1), and Fig. 2c shows the related accommodation of stress as a function of time. Cyclic plastic laws were identified from the stabilized stress-strain loops as the objective was to model high cycle fretting fatigue tests with crack nucleation time being always greater than $3x10^4$ cycles. All stress values were normalized by flat cyclic yield stress, $\sigma_{y,flat}$.

Extreme values of stabilized stress strain loop were plotted as a function of the corresponding deformation level on Fig. 2a for the flat material (32C1). These points were compared to the stress evolution of the tensile test. Considerable cyclic softening took place. Similar cyclic softening was observed for the cylinder material (FM35). For strains greater than 1%, experimental points showed progressive softening caused by damage. These points were not taken into account for the identification of the elastic-plastic law.

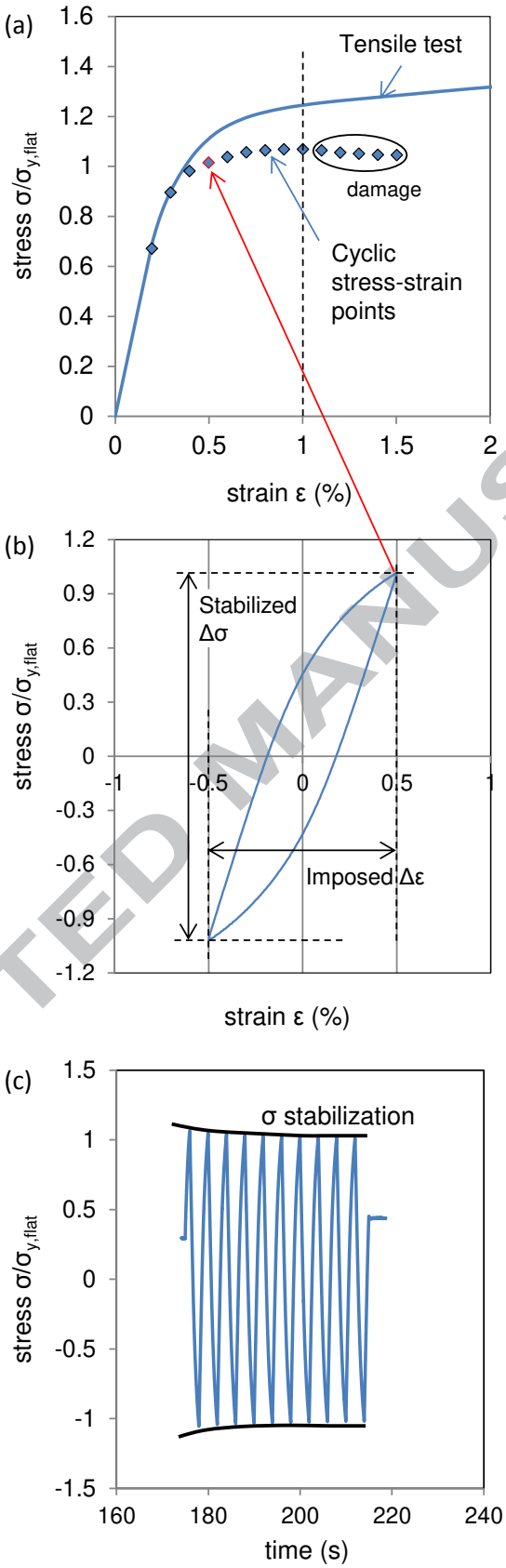

Fig. 2: 32C1 constitutive steel of flat material, cyclic and monotonic elasti-plastic behaviors. (a) (◆) Stabilized cyclic conditions compared to monotonic tensile test. (b) Stabilized stress-strain loop for 0.5% deformation level; (c) stress softening until stabilization with the applied cycles at 0.5% deformation level.

Cyclic stress evolution as a function of strain of Fig. 2a was modelled by two successive straight lines in order to identify a Prager linear kinematic hardening law. The parameters obtained are given in Table 2.

Fig. 3 compares the predicted stress-strain loops obtained with the linear kinematic hardening law for the flat material, versus the experimental loop at 0.5% strain. This linear description of hardening does not correlate perfectly with the experimental stress-strain loop. However, previous numerical analysis showed that a nonlinear kinematic law does not converge for small finite elements mesh size, as needed in fretting fatigue simulations. Linear description of hardening allows easier and faster modeling than nonlinear description while giving good lifetime predictions, as will be shown in this paper.

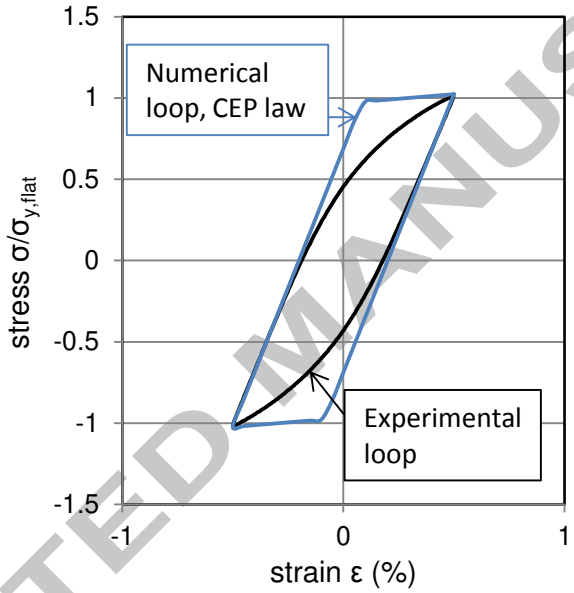

Fig. 3: Flat material 32C1 (deformation level: ε=0.5%): comparison of experimental stress-strain loop (▬) and numerical stress strain loop (▬) simulated with the cyclic law with linear kinematic hardening.

2.2 Fretting fatigue test device

The fretting fatigue test set-up is shown in Fig. 1b. Compared to plain fretting tests [20], fretting fatigue tests allow bulk fatigue loading, which helps propagate the cracks. Fretting fatigue experiments may lead to failure, while plain fretting cracks will always stop propagating due to high stress gradient below the contact: the further the crack is from the plain fretting contact surface, the more the crack driving force diminishes, to zero.

The fretting fatigue test machine comprised three actuators, for normal force P, fretting force Q and fatigue stress σ_F, respectively, as shown in Fig. 1b. This multiple actuator set-up allowed independent application of fatigue and fretting forces on the flat sample. In-phase sinusoidal cyclic tangential and fatigue forces were applied so that the maximum fretting load, Q^*_{max}, was applied at the same time as the maximum fatigue stress $\sigma_{F,max}$. During the test, displacement δ, normal force P and tangential force Q were recorded by multiple sensors, enabling the Q-δ fretting loop to be plotted and thus the fretting regime to be identified. As cracking was to be investigated, the displacements were kept small enough to maintain partial slip conditions. Frequency was fixed at 12 Hertz: high enough to investigate

a long test condition and low enough to guarantee test control stability. The fretting stress ratio was kept constant, at $R_Q = Q^*_{min}/Q^*_{max} = -Q^*/+Q^* = -1$.
Both constant and variable loading tests were carried out, with different fretting fatigue loading sequences, one after the other. In this study, only fretting and fatigue loading were changed from one block to another, while the normal force P was kept constant throughout the test.

2.3 Examination of fretting scars for unbroken specimens

After 10^6 cycles, if the fatigue sample had not failed, cracking was investigated using a destructive method. First, the sample was cut in the middle and then imbedded in epoxy to be polished to a mirror-like surface state. Next, cracks were observed by optical microscope. The polishing and observation steps were repeated two more times, so that crack measurement was performed on 6 different planes. Crack analysis was restricted to the middle of flat specimens, as the chosen dimensions allowed plane strain conditions along the central axis of the fretting scar. Similar crack lengths were observed in all 6 planes, and the maximum projected crack length b was determined. Fig. 4 shows an example of a fretting scar and the measure of the projected crack length b.

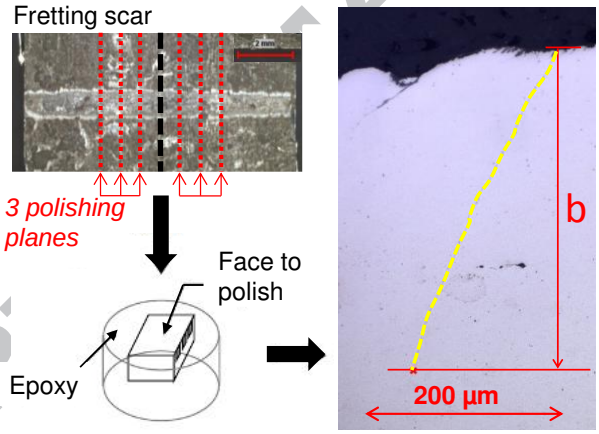

Fig. 4: Methodology for examining crack length in unbroken specimens.

2.4 Crack monitoring during test

Cracking status evolution in the fretting fatigue sample is usually unknown until end of test. As the present study objective was to predict cracking, experimental cracking data were needed for validation. For this, the potential-drop (PD) method was implemented on the fretting fatigue sample (Fig. 1c). PD provides direct information on crack propagation kinetics during testing, and was described in depth in refs [21,22]. A continuous current I=5A was applied through the fatigue test sample. Contact potential was measured between two Ø 0.1 mm platinum wires welded onto the sample surface. Potential was measured on each side of the sample to take account of the possible non-homogeneity in the crack. The measured potential depends on sample resistance. When a crack nucleates and propagates, sample cross-section diminishes and the electrical resistance of the uncracked cross-sectional area increases. Thus the measured PD increases.

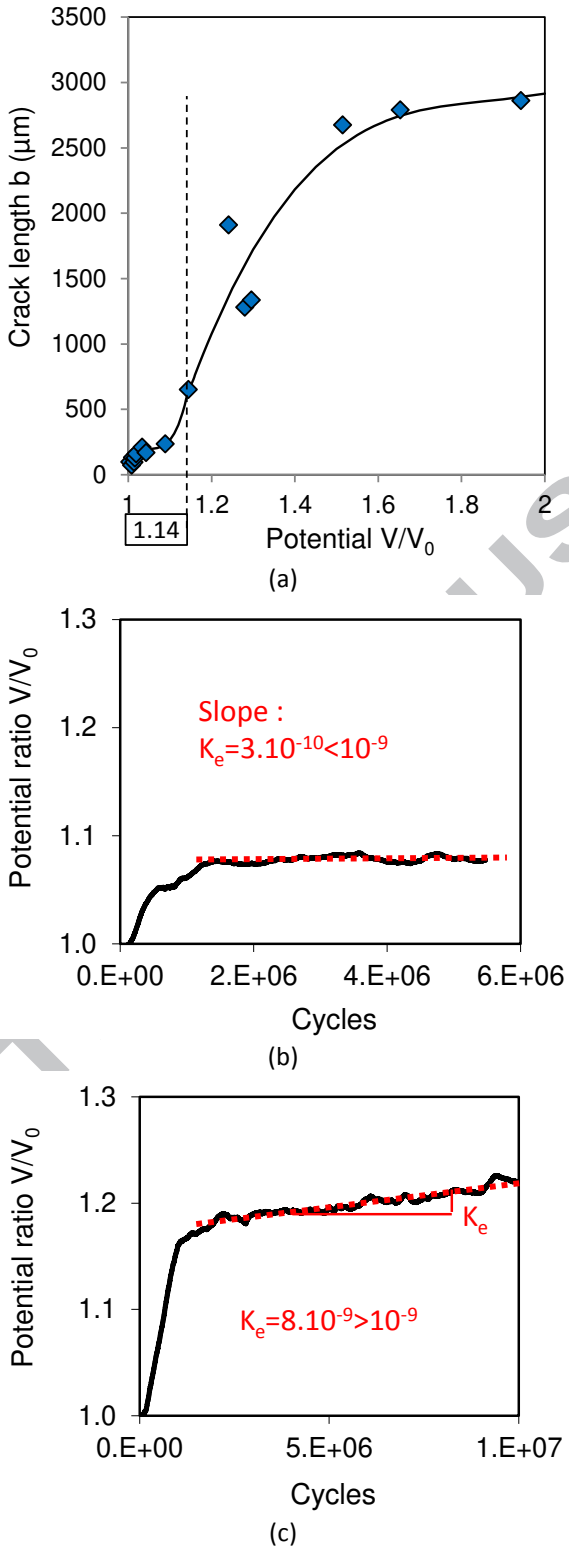

Fig. 5: (a) Calibration curve for a constant fretting fatigue loading (P, $\sigma_{F,mean}/\sigma_{y,flat}$=0.88, R_F=0.85, Q*/P=0.30). (b) Example of crack arrest condition as defined by the experimental crack arrest criterion based on the PD evolution slope. (c) Example of crack propagation condition as defined by the experimental crack arrest criterion based on the PD evolution slope.

A contact calibration curve was established by an empirical method (cf. Meriaux et al. [21]). For constant fretting fatigue stress of P, $\sigma_{F,mean}/\sigma_{y,flat}$ =0.78, R_F=0.85, and Q*/P=0.30, a dozen tests were carried out and were interrupted after varying numbers of fretting fatigue cycles.

Crack lengths were measured by the destructive method and plotted as a function of electrical potential (Fig. 5a). Potential values of each test were normalized by their respective initial value V_0.
Fig. 5a plots the calibration curve. Its evolution was complex, and was described by 2 successive polynomial functions:

For $1.01 < V/V_0 < 1.14$: $b = 643212.(V/V_0)3 - 2040300.(V/V_0)2 + 2157715.(V/V_0) - 760573$ (3)

For $1.14 > V/V_0$: $b = 5487.(V/V_0)3 - 30610.(V/V_0)2 + 57230.(V/V_0) - 33000$ (4)

Special care was taken to always position the probes at the same place, to limit scatter. However, the estimated crack length based on PD measurement depended on many variables, such as crack front shape, contact alignment and plasticity level [23]. Therefore, the fretting fatigue crack propagation rate estimated from inverse analysis of this calibration curve (i.e. b estimated from PD) should be taken with cautions, and crack extension analysis was based on the destructive method as far as possible.
However, the PD method appears to be a useful and consistent method for online estimation of crack arrest conditions. A crack propagation criterion was established from the slope of the potential K_e as a function of fretting fatigue loading cycles [22]: $K_e<10^{-9}$cycles^{-1} represents a crack arrest condition while, if $K_e>10^{-9}$cycles^{-1}, the crack is propagating. Examples of the application of this criterion for a crack arrest and a crack propagation situation are shown in Fig. 5b and Fig. 5c, respectively.

3 Predictive methodology for variable loading fretting fatigue tests

3.1 Finite elements analysis

Finite Elements Analysis (FEA) was carried out using Abaqus 6.10 software. A 2D plane strain model of the fretting fatigue test was generated (Fig. 6). Dimensions and boundary conditions matched the parameters of the physical experiment: i.e, the fretting fatigue sample was encased on the right while fatigue loading was applied on the left. The normal force was applied by pressing the cylinder pad on one side and the ball-bearing on the other side of the sample. No elements could rotate out of plane.
The loading blocks were applied directly one after the other, in the simulation as in the experimental test, thus taking account of the loading history in the stress field of each successive block.
Surface-to-surface discretization with small sliding was adopted for contact accommodation. The Lagrange multiplier was selected as the contact algorithm. The friction coefficient of the cylinder plane contact was determined experimentally, using the variable displacement technique described by Voisin et al. [24], μ=1.0. The contact between the ball-bearing and the fretting fatigue sample was considered frictionless.

The model was meshed with CPE3-type linear triangular elements, except in the contact zone, where CPE4R-type linear quadrilateral elements were used; this zone was also meshed more densely than the other regions (from 10 µm near the contact to 50 µm deep in the

sample). Stress convergence in a similarly meshed model was investigated in a previous study [18], which showed that consistent crack nucleation predictions could be obtained if the stress analysis exclusively involved subsurface stress components, defined at the second node and further below the surface (in the present case, z≥20µm). The 10µm mesh size chosen for the contact allowed better convergence, saved considerable computation time and was small enough compared to the critical distance that was used. A structured mesh is also necessary for accurate crack propagation prediction. 50µm quadrilateral elements were implemented in the volume, to achieve a good compromise between computational cost and crack propagation increment.

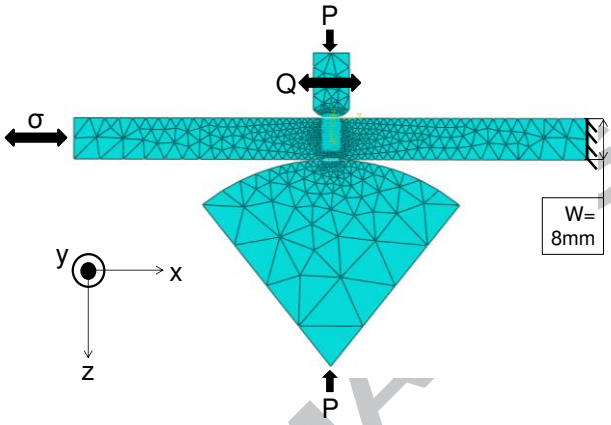

Fig. 6: Finite elements model of the fretting fatigue test (rotated 90° to the right compared to the experimental test device).

The normal force P was high enough to generate plasticity. The added fatigue loading enhanced plasticity. Consequently, cylinder and fatigue sample behaviors were well described by the cyclic elastic-plastic (CEP) laws introduced in section 2.1. Activated plasticity decreased after each cycle, due partly to material hardening but mostly to plastic accommodation of the contact geometry (Fig. 7). Numerical analysis showed that macro contact accommodation, which is accommodation of contact half-size, occurred quickly after around 10 loading cycles (Fig. 7a and d), with contact half-size increasing by 15%.

Local stabilization of the material took much longer. It was quantified by assessing the most highly strained integration point (Fig. 7a). Two methods were applied: in terms of stress-plastic strain loop evolution (Fig. 7b), shakedown corresponds to the time from which loops became closed and vertical; alternatively, in terms of increase in plasticity (Fig. 7c), shakedown corresponds to the beginning of the horizontal evolution. In the case studied in Fig. 7, material local accommodation was achieved after around 150 loading cycles. This accommodation time may vary with loading amplitude and the constitutive law. It should be noted that elements around the contact border reached elastic shakedown earlier.
Comparison with the evolution of both, p_{max}, the maximum contact pressure, and q_{max}, the maximum surface shear, stresses, which stabilized after 10 numerical cycles (Fig. 7d), suggests that contact loadings were mainly driven by extension of the plastic contact area rather than by the material plastic response.
Fatigue analysis to predict cracking in variable loading test sequences was therefore performed on the stable elastic shakedown state. All simulations ran for 100 numerical cycles for crack nucleation conditions and 200 cycles for crack propagation conditions, which was about 2h long. Computation time may seem long, but the model used a very fine mesh

and was still much quicker than experimental testing. Lifetime study was then performed, distinguishing crack nucleation life and crack propagation life.

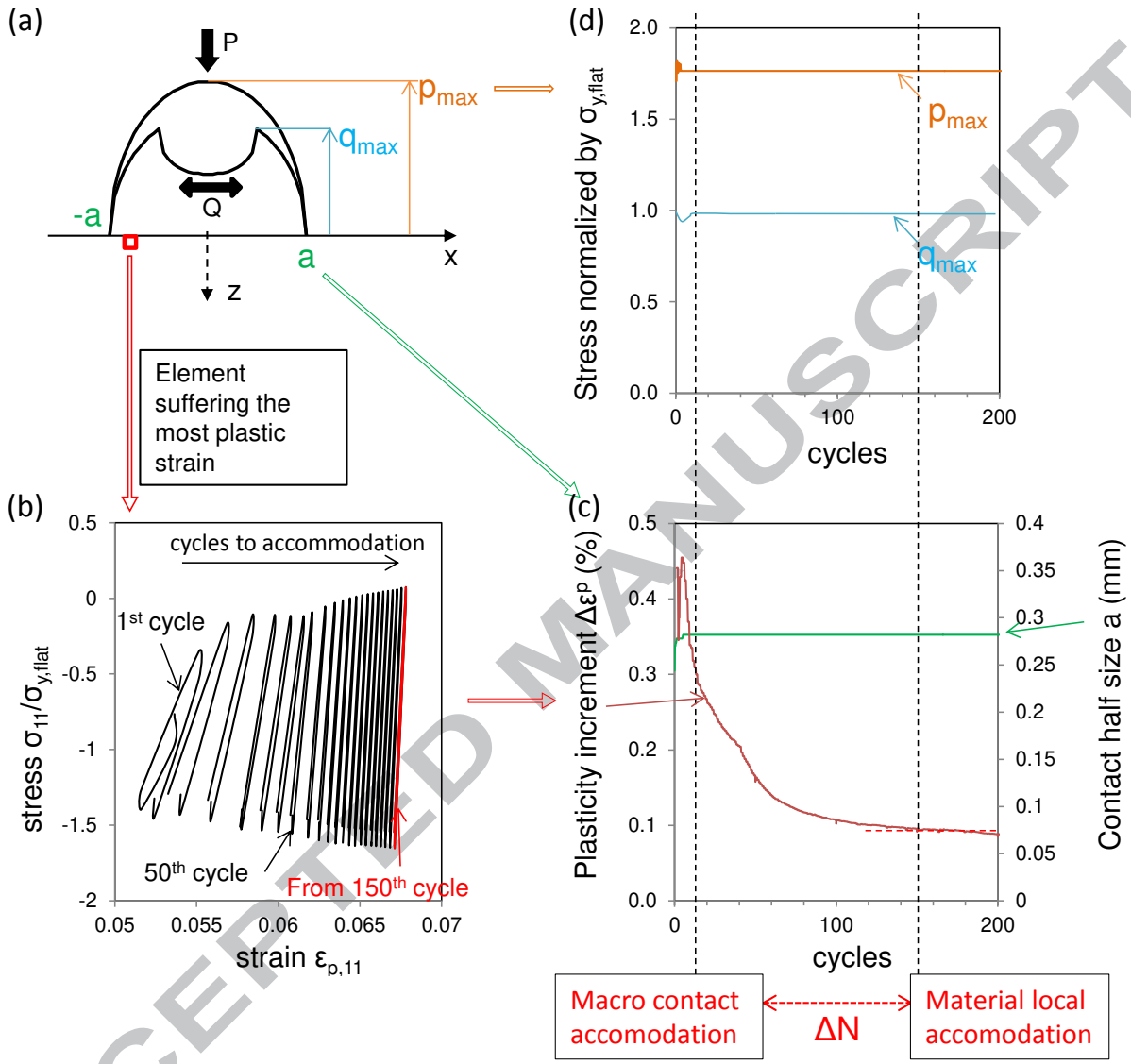

Fig. 7: Evolution of a fretting fatigue contact subjected to the loading P, $Q^*/P=0.3$, $\sigma_{F,mean}/\sigma_{y,flat}=0.88$, $R_F=0.85$ for 200 numerical cycles to characterize elastic shakedown. (a) Diagram of the contact; (b) evolution of the stress-plastic strain loops of the most plastic strained element; (c) evolution of $\Delta\varepsilon^p$ of the most plastic strained element compared to contact half-size evolution; (d) related evolution of p_{max} and q_{max} contact stresses.

3.2 Crack nucleation life

3.2.1 Crossland crack nucleation criterion

As it is well adapted for formalizing the multiaxial infinite endurance of steel, Crossland's multiaxial fatigue criterion was used to identify the crack nucleation condition. Crossland's criterion expresses cracking risk as a linear combination of the maximum amplitude of the second invariant of the stress deviator defined by $\sqrt{J_{2,a}}$, and the maximum value of the hydrostatic pressure $\sigma_{H,max}$ [25]. Crossland equivalent stress σ_C is expressed as:

$$\sigma_C = \sqrt{J_{2,a}} + \alpha.\sigma_{H,\max} \quad (5)$$

where

$$\sigma_{H,\max} = \max_{t\in T}\left(\frac{1}{3}trace\left(\underline{\underline{\Sigma}}(t)\right)\right) \quad (6)$$

$$\sqrt{J_{2,a}} = \frac{1}{2}\max_{t_0\in T}\left\{\max_{t\in T}\left[\frac{1}{2}\left(\underline{\underline{S}}(t)-\underline{\underline{S}}(t_0)\right):\left(\underline{\underline{S}}(t)-\underline{\underline{S}}(t_0)\right)\right]^{1/2}\right\} \quad (7)$$

$$\alpha = \frac{\tau_d - \frac{\sigma_d}{\sqrt{3}}}{\frac{\sigma_d}{3}} \quad (8)$$

with S the deviatoric part of Σ, σ_d the traction-compression fatigue limit (R_F=-1) and τ_d torsion fatigue limit (R_F=-1).

The α coefficient was established from alternating shear and tensile fatigue limits at 10^6 cycles: σ_d=0.70x$\sigma_{y,flat}$ and τ_d=0.51 x$\sigma_{y,flat}$. A previous study showed very low fluctuation according to N, and thus the α coefficient was considered constant: α(N)=α=0.46±0.02.
Cracking risk could then be estimated by comparing Crossland equivalent stress with the alternated torsion fatigue limit: when

$$\sigma_C \geq \tau_d \quad (9)$$

there is a risk of cracking.

3.2.2 Application of Crossland's criterion to predict infinite fretting fatigue endurance

Fig. 8a plots the subsurface distribution of Crossland equivalent stress related to the fretting fatigue crack nucleation condition: P, Q*/P=0.13, $\sigma_{F,mean}/\sigma_{y,flat}$=0.88, R_F=0.85. It shows severe stress gradient at the hot spot (i.e., the top surface contact border in fretting fatigue), which comes from the fretting contact loading. Stress gradients lead to over-conservative estimation of cracking risk at the hot spot. This behavior is well known and usually taken into account by using non-local fatigue stress analyses such as mean volume, mean distance or critical distance analysis [20,26–28].

We focused on the critical distance method. Hence, instead of considering the surface hot-spot stress at the surface trailing contact border, fatigue analysis was performed at a critical distance (ℓ) below the surface, vertical to the hot spot stress contact border (x=-a, z=ℓ)(Fig. 8b). The question was: which critical length ℓ to consider?

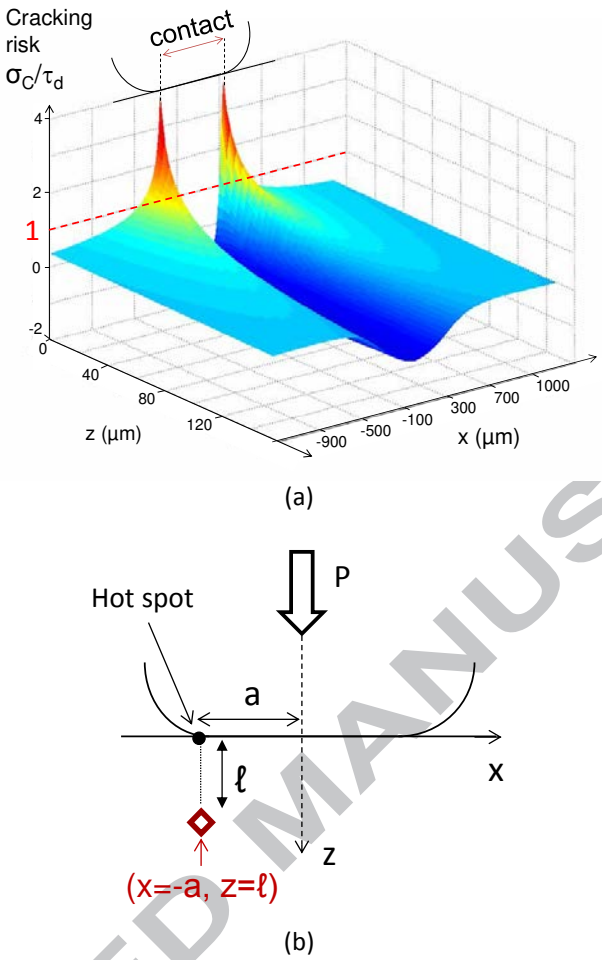

Fig. 8: (a) Subsurface distribution of Crossland cracking risk. (P, Q*/P=0.13, $\sigma_{F,mean}/\sigma_{y,flat}$=0.88, R_F=0.85). (b) Principle of the critical distance method.

In a previous paper, we sought to optimize the critical distance strategy by clarifying the influence of crack length on crack nucleation prediction [18]. For a given fretting fatigue contact (R, P), there was shown to be an optimal (ℓ_{opt}-b_{opt}) condition in which cracking risk prediction error was minimal, with ℓ_{opt} the optimal critical distance related to the optimal crack nucleation length b_{opt}.
Considering several patterns of crack nucleation threshold evolution related to various loadings, for each crack length from 0 µm to 100µm, the related critical distance was calculated by inverse analysis. Then, for each possible crack nucleation length b, the mean critical distance $\overline{\ell}$ and standard deviation $\mathrm{SD}(\ell)$ were plotted as a function of crack length in Fig. 9.

The standard deviation showed a remarkable bell shape, with a clear minimum for b=60µm. This suggests that crack nucleation has to be calibrated with respect to a representative incipient crack length for which prediction error is minimal. If the chosen crack length is too small (i.e., b<60µm), it is probably not representative of a damaging crack, since such very small cracks may never propagate. By contrast, if the chosen crack length is too long (i.e., b>60µm), it is probably partly governed by crack propagation rather than pure crack nucleation. Hence, there is an optimal pairing of crack initiation length and critical distance (ℓ_{opt}-b_{opt}) for which crack nucleation prediction is optimal (Fig. 9): ℓ_{opt}=25µm and b_{opt}=60µm.

It is interesting to note that $\ell_{opt}=b_{ø}/2$ with $b_{ø}=50\mu m$ represents the transition from short-to-long crack, which confirms Taylor's theory [26]. Identifying this ℓ_{opt}-b_{opt} couple is time consuming, needing lots of experimental results; the following axiom was therefore considered:

- $\ell_{opt}=b_{ø}/2$, with $b_{ø}$ the short-to-long crack transition as defined by the Kitagawa-Takahashi diagram [29];
- $b_{opt}= b_{ø}$.

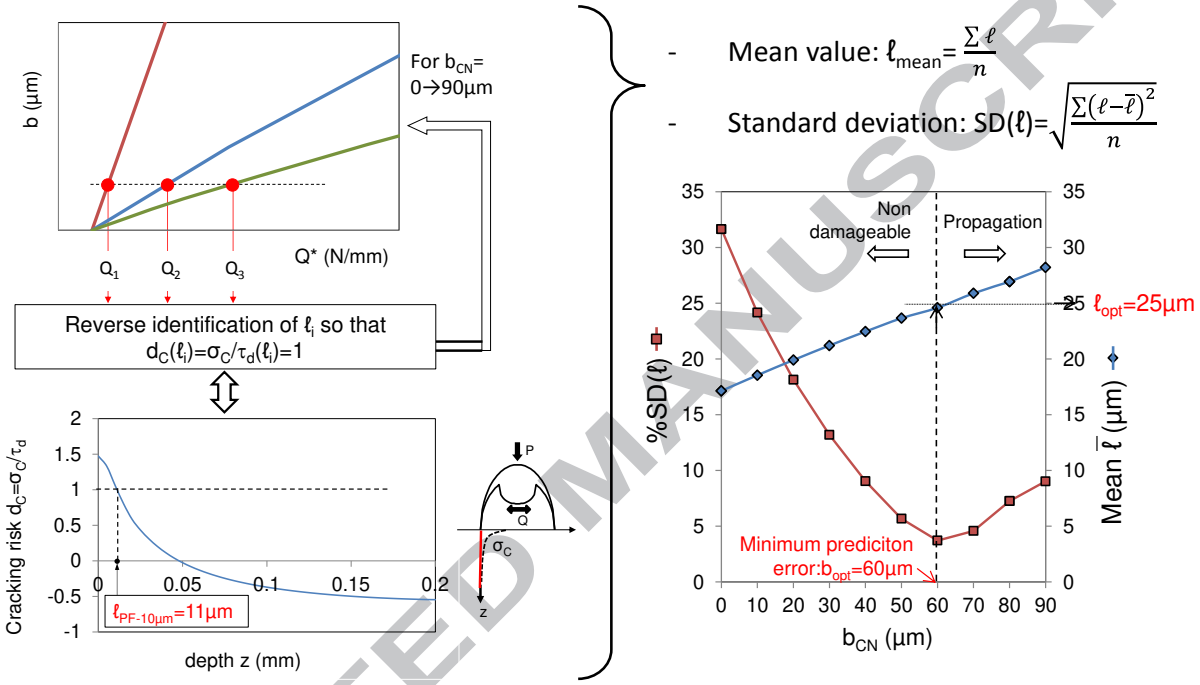

Fig. 9: Identification of optimal (ℓ_{opt}-b_{opt}) couple to predict crack nucleation, following the method of section 3.2.2 which is further developed in [18].

Following this strategy, a given fretting fatigue loading nucleates a crack if the equivalent Crossland stress located at a critical distance $\ell_{opt}=25\mu m$ under the hot spot is greater than or equal to τ_d (Equation 9). In addition, the nucleated crack length will be equal to $b_{ø}$.
It should be noted that, since the crack nucleation length corresponds to the short-to-long crack transition, propagation prediction is made easier by not having to consider the short crack propagation regime to predict fretting fatigue endurance.

3.2.3 Predicting crack nucleation endurance

Crack nucleation prediction as described above corresponds to infinite endurance. To predict crack nucleation endurance, the criterion must be adapted as a function of the number of cycles. A set of plain fretting experiments was performed, using the same contact configuration, to identify $Q^*_{CN}(b_{opt},N)$, the tangential forces inducing a crack nucleation length of b_{opt} for different test durations (Fig. 10a and b).

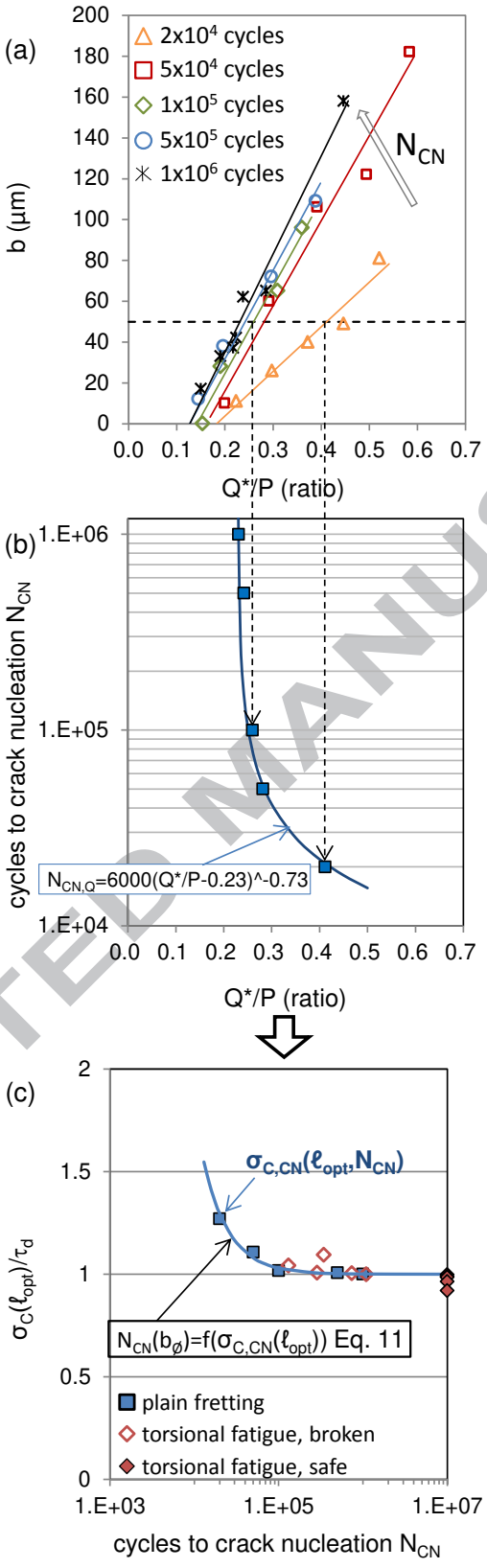

Fig. 10: Methodology used to identify crack nucleation endurance from reverse analysis of plain fretting cracking experiments. (a) Crack extension for different plain fretting test durations (b assessed using a destructive method; P, R=4.6mm, 12Hz; △: $2x10^4$cycles; □: $5x10^4$cycles; ◇: $1x10^5$cycles; ○: $5x10^5$cycles; ✳: $1x10^6$cycles. (b) Evolution of tangential force nucleation endurance $Q^*_{CN}(b=b_ø;N_{CN,Q})$. (c) Identification of crack nucleation endurance from reverse plain fretting analysis (■): identification of $N_{CN}(b_ø)$ (▬) Eq. 11 and comparison with torsional fatigue experiments (◇: broken, ◆: safe).

From this analysis, crack nucleation endurance could be expressed using a power law formulation (Fig. 10b):

$$N_{CN,Q}=A_1 \left(\frac{}{P}\right) Q^{b_1} \quad (10)$$

with A_1=6000, b_1=-0.73 and Q_∞=0.23 for $\ell_{opt}= b_\phi /2$=25µm and $b_{opt}= b_\phi$=50µm.
Then each crack nucleation condition $Q^*_{CN}(b_\phi,N)$ was simulated to extract the corresponding $\sigma_{C,CN}(\ell_{opt},N)$, Crossland equivalent stress at the optimal critical distance (Fig. 10c). Again, a power law could be formulated:

$$N_{CN}(b_\phi)=A \quad (11)$$

with $\ell_{opt}=b_\phi/2$, $A_2=8.5x10^3$ and b_2=-0.7.

These data were compared to the alternative shear fatigue endurance data (Fig. 10c). Although the critical distance approach was calibrated using 10^6 cycles fatigue limits, correlation with the HCF shear endurance curve was very good, at least in the high-cycle fatigue domain (N>5.10^4 cycles).

This implicitly supports applying the proposed (ℓ_{opt}-b_{opt}) concept and reverse plain fretting cracking analysis to calibrate crack nucleation rate under severe stress gradient conditions as in fretting fatigue contact. The endurance curve determined, fretting fatigue crack nucleation (related to $b=b_\phi$) is predicted by solving the following relationship at the contact border (x=-a):

(12)

with $\sigma_{C(FF),CN}(\ell_{opt}, N_{CN})$ fretting fatigue crack nucleation condition and plain fretting crack nucleation condition from the endurance curve obtained by reverse analysis.

Variable loading tests require a damage accumulation rule if the crack does not nucleate in the first block. The simple linear Miner model was chosen for its straightforwardness [30]. After each loading increment ΔN, damage increment ΔD_i related to i, the loading condition, was computed so that:

$$= \frac{\Delta N}{N_{CNi}} \quad (13)$$

with N_{CNi} the crack nucleation endurance related to the fretting fatigue loading condition of block i

$$N_{CNi}=A \quad (14)$$

The linear Miner damage model states that that a crack of length $b_{opt}= b_{ø}$ nucleates when total damage D:

$$D = \sum D_i = 1 \quad (15)$$

3.3 Crack propagation prediction

Once a crack is nucleated, it may propagate. Crack nucleation length being equal to $b_{ø}$, with $b_{ø}$ the short-to-long crack transition as defined by the Kitagawa-Takahashi model [29], crack propagation prediction was simplified by eliminating the short-crack propagation regime.
An uncoupled approach was used to predict crack propagation. First, the contact stress state was obtained by finite elements modeling (FEM) combining the cyclic elastic-plastic law, then the normal stress along the expected crack path was determined at the contact border for the maximum and minimum loading conditions, as schematized in Fig. 11a.

Then the mode I stress intensity factor (SIF) K_I was calculated, using Bueckner weight function approach [31] (Fig. 11b):

$$\mathrm{K_I} = \sqrt{\frac{2}{\pi}} \int_0^{\mathrm{h}} \mathrm{M(t).}\,\sigma_{\mathrm{x}}(\mathrm{t})\mathrm{dt} \quad (16)$$

with

$$\mathrm{M(t)} = \mathrm{t}^{-1/2}.\left[1 + \mathrm{m_1}.\frac{\mathrm{t}}{\mathrm{h}} + \mathrm{m_2}.\left(\frac{\mathrm{t}}{\mathrm{h}}\right)^2\right] \quad (17)$$

$$\mathrm{m_i} = \mathrm{A_i} + \mathrm{B_i r^2} + \mathrm{C_i r^6} \quad (18)$$

$A_1=A_{ref}$, $B_1=27.9558A_{ref}$, $C_1=14.2870A_{ref}$, $A_2=0.4070A_{ref}$, $B_2=5.3504A_{ref}$ et $C_2=113.9489A_{ref}$.

The contribution of mode II was neglected: Fouvry et al. [32], followed by De Pannemaecker et al. [33], demonstrated that the K_I value from a crack normal to the contact surface with a mode I formulation gives a value very close to the mixed mode I and II stress intensity factor of a kinked crack. Mode II affects crack propagation only for the first dozens of microns below the surface.
It is important to note that the weight function strategy can result in a negative K_{Imin} value, which has no physical meaning (Fig. 11b). The minimum physical K_I value is $K_I=0$, as crack lips are closed under compressive stress and the material response is theoretically equivalent to that of an uncracked specimen [34]. Nevertheless, an important point to consider is that the complexity of the fretting contact zone involves large stress gradients, leading to variation in the stress ratio below the surface, which has to be taken into account. Following the strategy developed in [34,35], results were compiled versus the SIF ratio $R_K=K_{Imin}/K_{Imax}$ (Fig. 11c).

To take account of variation in R_K ratio as shown in Fig. 11c, equivalent stress or effective stress intensity factors were used to study crack propagation. In this paper, Kujawski's fatigue crack driving force parameter was considered [36] (Fig. 11d):

$$\overline{K}^{*}=(\Delta K^{+})^{0.5}.K_{Imax}{}^{0.5} \quad (19)$$

with $\Delta K^+ = \Delta K = K_{Imax}-K_{Imin}$ for $R_K>0$ and $\Delta K^+=K_{Imax}$ for $R_K\leq 0$. Note that, with this description, both ΔK^+ and $\overline{K}^*$ are always greater than or equal to zero.

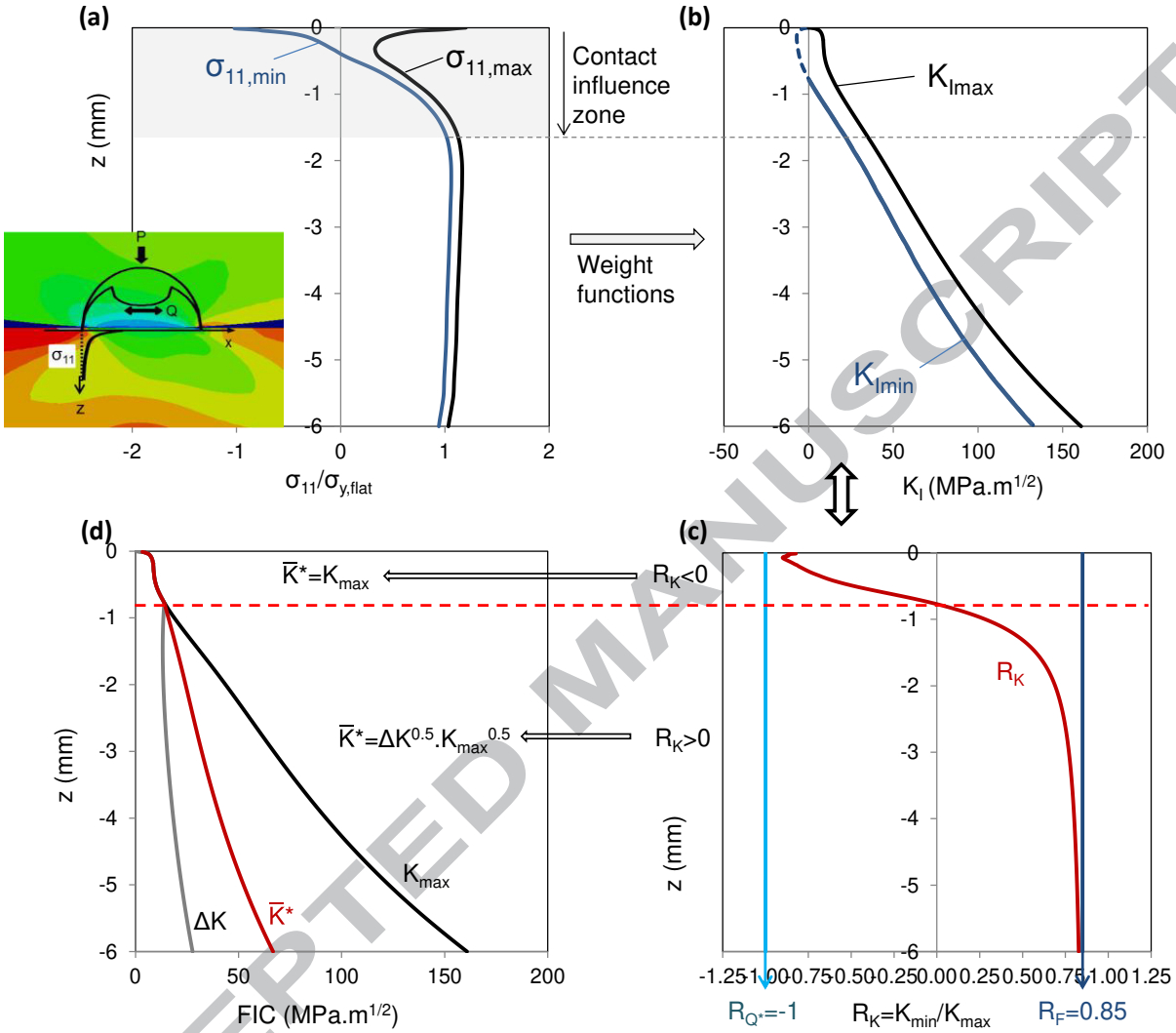

Fig. 11: (a) $\sigma_{11,max}$ and $\sigma_{11,min}$ evolutions as a function of depth extracted from stabilized elastic-plastic FE simulation at x=-a. (b) Related K_{Imax} and K_{Imin} evolutions estimated with weight functions from the FE stresses. (c) $R_K=K_{min}/K_{max}$ as a function of depth; (d) corresponding $\overline{K}^*$ paremeter in the depth of the sample. P, $\sigma_{F,mean}/\sigma_{y,flat}$=0.88, R_F=0.85, Q*/P=0.30.

The loading cycles related to the propagation stage were finally computed using Kujawski's $\overline{K}^*$ fatigue-crack-driving force parameter, coupling the Paris law of the material:

$$N_P = \int_{b=b_0}^{b_{failure}} \frac{db}{C\overline{K}^{*m}} \quad (20)$$

The Paris propagation law parameters were obtained from conventional 4-point bending tests; $C=5.35\times10^{-10}$ and m=3.26.

Failure was related to $K_{Imax}=K_{IC}$, with K_{IC} critical stress intensity factor K_{IC}=212MPa. Alternatively, if $\overline{K}^*(b)$ crosses the crack arrest condition ΔK_{th}, then the crack stops propagating and crack arrest is reached if:

$$\overline{K}^*(b) \leq \Delta K_{th}(b) \quad (21)$$

The threshold crack arrest condition is defined using El Haddad's continuous model [37]:

$$\Delta K_{th} = \Delta K_{\emptyset}\sqrt{\frac{b}{b+b_{\emptyset}}} \quad (22)$$

with $b_{\emptyset}$=50µm the short to long crack transition and $\Delta K_{\emptyset}$=6.3 MPa.m$^{1/2}$ the long crack threshold previously defined by reverse identification on plain fretting experiments [16].

3.4 Global predictive method

The global process to estimate cracking under constant conditions or variable loading sequences was as follows:

- Firstly, fretting fatigue loading was simulated by finite elements analysis.
- Secondly, Crossland cracking risk $\sigma_C(x=-a,z=\ell_{opt})$ was calculated at the end of each loading sequence. The corresponding crack nucleation endurance of each block N_{CNi} was estimated using Eq. 11.
- Thirdly, $\overline{K}^*(z)$ for each loading sequence was calculated from the stabilized stress at the contact border.
- Finally, N_{CNi}, K_{Imax} and $\overline{K}^*$ were entered in the predictive algoritm presented in Fig. 12, to estimate the cracking process.

Other necessary inputs are b_{opt}, which is equal to $b_{\emptyset}$, and K_{IC} and ΔK_{th}. These material parameters may be estimated by reverse identification on a few plain fretting experiments [16].

The algorithm begins by estimating crack nucleation endurance using the linear Miner damage law. Two outcomes are possible: either no crack is nucleated at the maximum number of cycles allowed for the algorithm, or a crack is nucleated with crack length $b_{\emptyset}$ at N_{CN}. If a crack is nucleated, propagation is predicted. If crack arrest is detected, the algorithm jumps directly to the next loading sequence. Three outcomes are then possible: either there is failure at N_T with $N_T=N_{CN}+N_P$, or there is crack arrest at end of test, or the crack is still propagating at the maximum number of cycles provided for in the algorithm.

It should be noted that the evolution of b and N is recorded as the algorithm progresses, which allows theoretical cracking to be plotted as a function of the number of cycles.

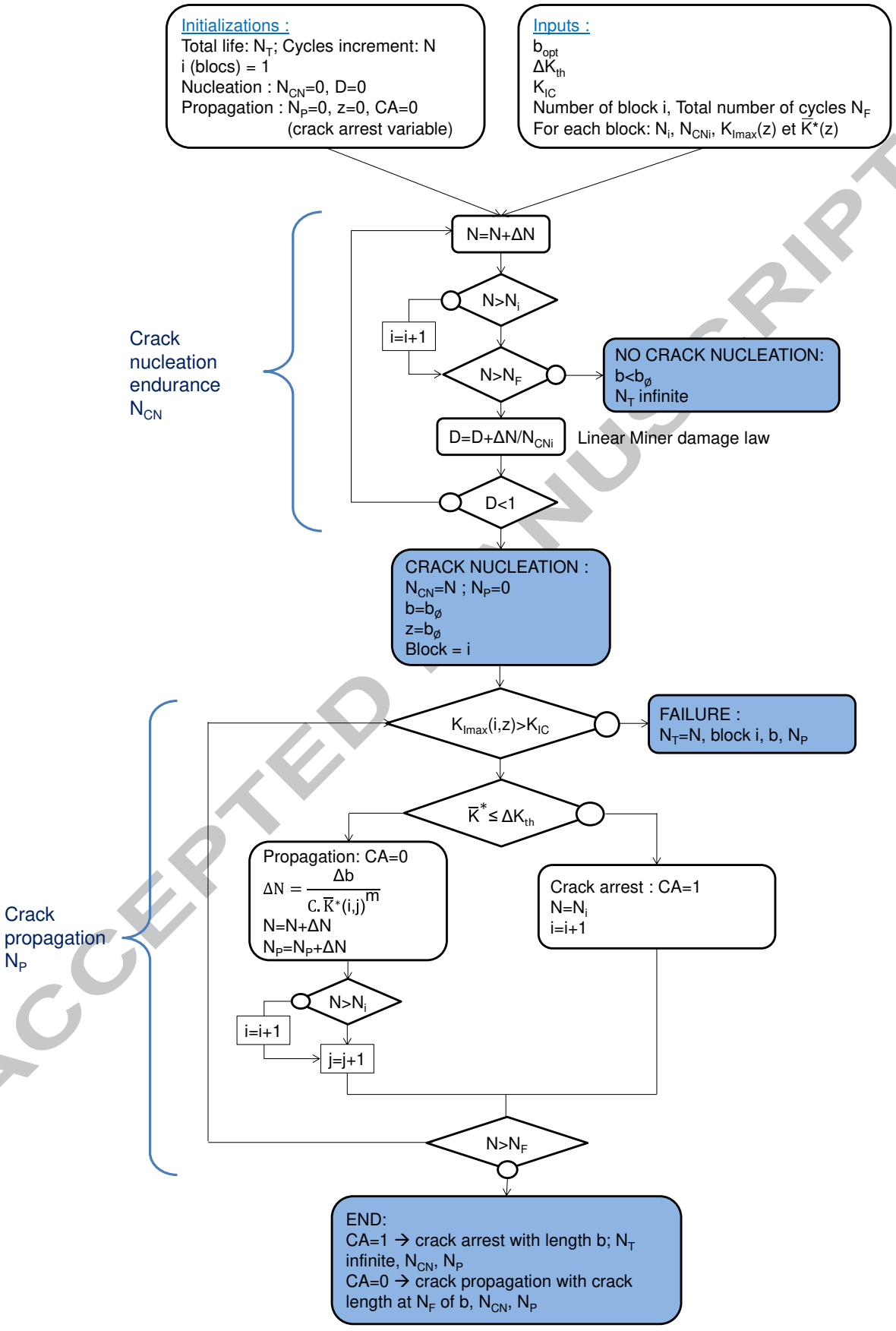

Fig. 12: Lifetime estimation process.

4 Comparison between experiments and prediction

4.1 Constant loading conditions

Three individual fretting fatigue loadings, A, B and C, were considered (Table 3). Fig. 13 plots PD evolution for each loading applied individually to the fretting fatigue contact described in section 2.1.

Table 3: Individual fretting fatigue loadings applied in the variable loading tests

Loading	Color code	$\sigma_{F,mean}/\sigma_{y,flat}$	R_F	Q*/P	N
A: Max		0.88	0.85	0.3	70000
B: Mean		0.88	1	0.38	670000
C: Min		0.99	0.85	0.15	1000000

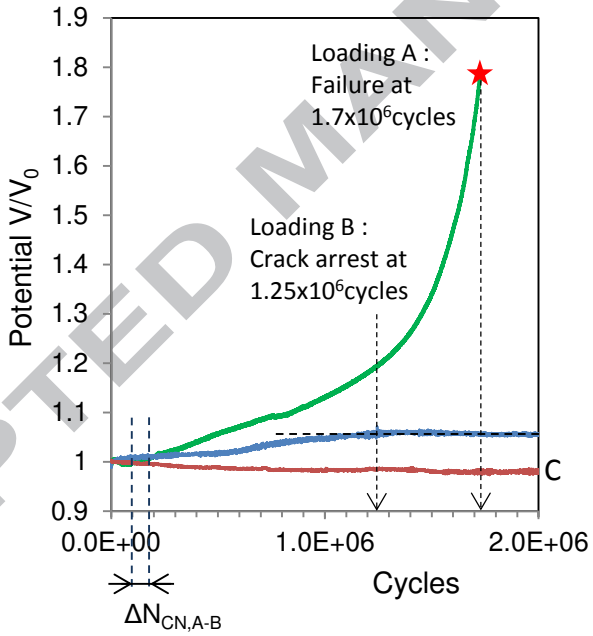

Fig. 13: PD evolution of each loading in Table 3.

Using the calibration curve, estimated length extension is compared to prediction in Fig. 14. Theoretical modeling seemed consistent with the experimental results. Loading condition C, with the lowest fretting stress, showed a flat or even decreasing evolution of PD, suggesting no crack nucleation. Cross-section examination showed a very small crack length of b_C=40µm, below the $b_ø$ crack nucleation threshold. This result was predicted by the model, according to which, for fretting fatigue loading case C, the Crossland stress $\sigma_C(\ell_{opt})/\tau_d$=0.78 remains smaller than the τ_d crack nucleation condition.

By contrast, loading case A, with the highest fatigue stress and medium fretting loading, nucleated quickly and then propagated until failure at $N_{F(A)}$=1.7x10^{6}cycles. This evolution was well predicted by the model, with $b_ø$ crack nucleation predicted at $N_{CN(A),th}$= 19 200 cycles and failure at $N_{F(A),th}$= 1.01x10^6 cycles.

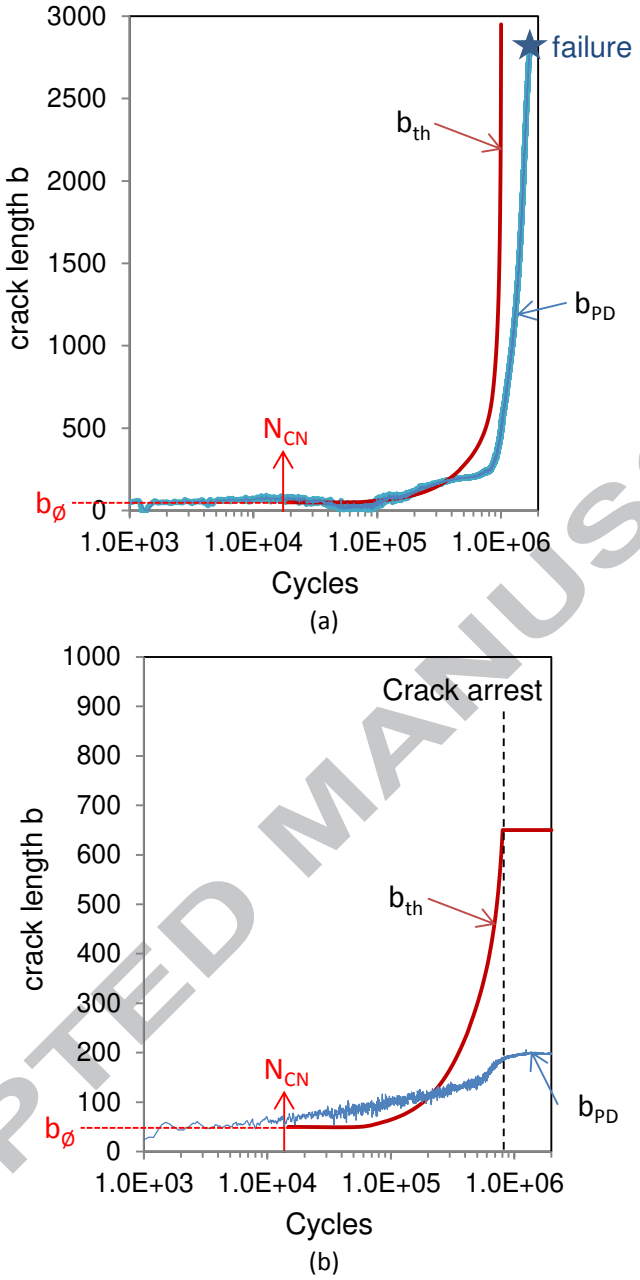

Fig. 14: Comparison of crack length extension related to (a) fretting fatigue loading A, and (b) fretting fatigue loading B.

Loading condition B, with the highest fretting stress and low fatigue stress (R_F=1), induced crack nucleation due to contact stress, followed by crack arrest (K_e<10^{-9}) due to constant bulk stress. A maximum crack length of $b_{CA(B),exp}$=215µm was found after cross-section examination, and the crack arrest condition (i.e. beginning of plateau evolution) was estimated at $N_{CA(B),th}$=1.2x10^6 cycles. This typical evolution was again well predicted by the model. Crack nucleation endurance was predicted at $N_{CN(B),th}$=14 800 cycles, crack arrest at 0.8x10^6cycles and crack arrest length at $b_{CA,th(B)}$=650µm. The predicted crack extension was too conservative; however, this is consistent with the safety margin needed in industry.

The first investigation of constant fretting fatigue conditions confirmed the reliability of the model in predicting no nucleation, crack nucleation followed by crack arrest, or failure.

Reasonably consistent estimates of crack length and fretting fatigue endurance were also obtained. The next step of analysis was to assess predictions for variable block loading sequences.

4.2 Variable loading sequences

The previous 3 loading sequences were mixed to study 3 different variable loading conditions, as schematized in Fig. 15, where fretting tangential force Q and fatigue stress σ sequences are superposed. The number of cycles associated with each loading was reduced so as to have a final test lasting a reasonable time (c.f. Table 3): N_F=1.74x10^{6}cycles, comprising N_A=7x10^{4}cycles, N_B=6.7x10^{5}cycles and N_C=1x10^{6}cycles. These new numbers of cycles were kept constant from one variable loading test to another. Each condition was performed experimentally and compared to predicted crack length extension.

To evaluate loading evolution, the $\sigma_C(\ell_{opt})$ stress parameter was computed. This stress analysis suggested that the (B,A,C) loading sequence induced a decrease in the $\sigma_C(\ell_{opt})$ stress path, the (C,A,B) sequence a rising $\sigma_C(\ell_{opt})$ response, and the (A,B,C) loading sequence a mixed $\sigma_C(\ell_{opt})$ evolution. Note that this stress description was based on a crack nucleation stress description and did not consider the crack extension process, which is more complex to address.

4.3 Decreasing $\sigma_C(\ell_{opt})$ stress path evolution: (B,A,C) sequence

This case could be expected to produce the worst damage. It is widely agreed that decreasing loading, by fostering early crack nucleation, increases damage. Fig 15a plots the potential evolution of the decreasing load case. The crack nucleated at the first loading block and propagated until failure in block 3. A similar evolution was well predicted by the model.
This result may seem surprising, as the C loading sequence produced only a small crack when applied individually, but may be explained by looking at the details of crack propagation provided by the algorithm.

Fig. 15a shows that the first loading block, B, nucleated a crack after 3x10^4 fretting fatigue cycles, corresponding to 4% of the number in cycles of the block. Crack nucleation was expected from the individual behavior of loading B, even if the crack nucleation criterion overestimates crack nucleation life.
Once the crack was nucleated, it continued propagating in the first block, as depicted in Fig. 15a. Crack propagation from one loading block to the next was determined by considering $\overline{K}^*$ at the end of each loading block combined with the Paris law. Fig. 16a shows how the algorithm navigated from one $\overline{K}^*$ block evolution to another in the first, second and third blocks. At the end of the first block, the algorithm already predicted a crack of 500 µm. Then, when the second block was applied (loading A), the crack propagated greatly despite the short number of cycles. Hence, when the third sequence (loading C) was finally applied, the crack was long enough to be outside of the crack arrest zone of the loading (Fig. 15a). This means that an apparently harmless loading condition may propagate a crack and lead to failure if the initial cracking defect is large enough. The algorithm predicted failure at $N_{T(th)}$=1 347 000 which was very close to the experimental lifetime of $N_{F(exp)}$=1 520 000 cycles.

The evolution of predicted crack length was also compared to the experimental evolution given by the PD measurements (Fig. 15a). The model seemed to overestimate crack propagation; however, it is difficult to draw any conclusion from this condition alone.

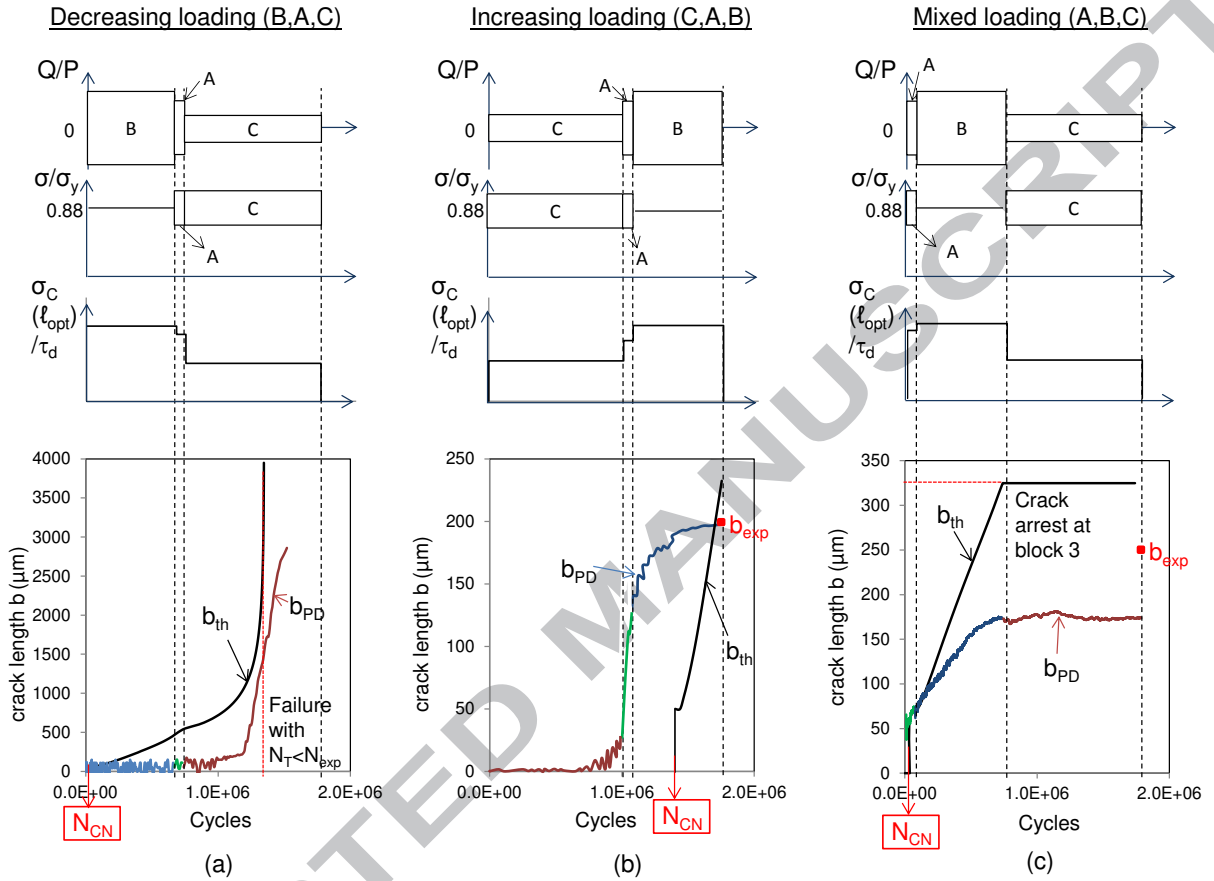

Fig. 15: Experimental PD evolution compared with theoretical predicted cracking behavior as a function of number of cycles for (a) decreasing loading, (b) increasing loading case and (c) mixed loading case. N_A=7x10^4 cycles, N_B=6.7x10^{5}cycles, N_C=1x10^6 cycles: i.e., N_F=1.74.10^6 cycles. For loadings, see Table 3.

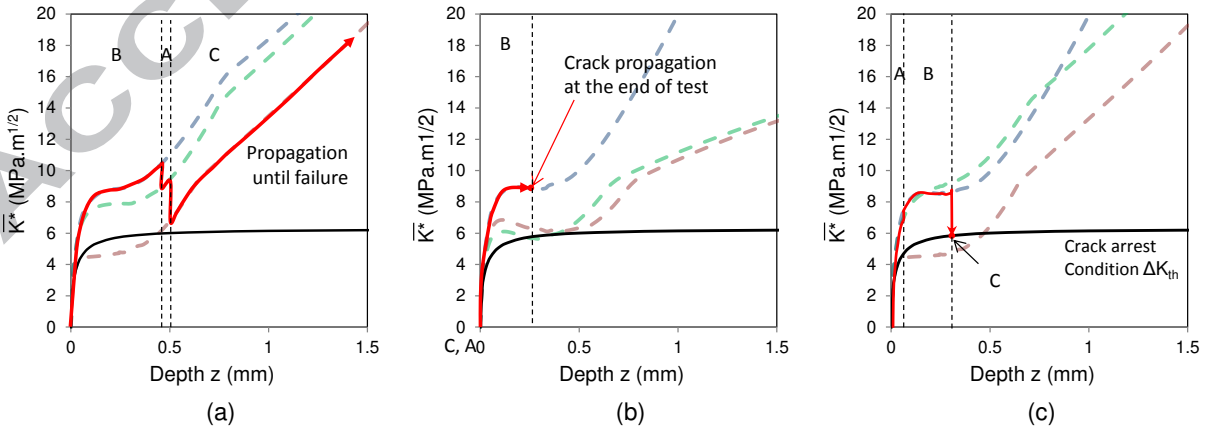

Fig. 16: Progression of the crack propagation algorithm for (a) decreasing loading, (b) increasing loading and (c) mixed loading. N_A=7x10^4 cycles, N_B=6.7x10^{5}cycles, N_C=1x10^6 cycles: i.e., N_F=1.74.10^6 cycles. For loadings, see Table 3.

4.4 Increasing $\sigma_C(\ell_{opt})$ stress evolution: (C,A,B) sequence

Fig. 15b plots experimental crack evolution according to the PD method and predicted crack propagation length according to the algorithm for the increasing loading case.
Potential evolution showed that crack nucleation happened in the third block at $N_{CN}=1.4x10^6$ cycles. This was surprising, as crack nucleation seemed to happen during the second sequence according to potential-drop evolution (Fig. 15b). In addition, second-sequence loading (loading A) was high enough to produce crack nucleation even within a small number of cycles. In this case, strong plastic accommodation acquired during previous loadings led to a softening of stress during the second sequence, and the number of cycles was not enough to nucleate a crack. Accordingly, crack nucleation occurred at 49% of the last block, which is much longer than when block B was applied alone. Once again, plastic accommodation led to softening of the stress field.

The potential slope K_e was still greater than 10^{-9} at end of test (that is, end of third loading sequence). Following the experimental crack arrest criterion detailed in section 2.4, this indicates that the crack was still propagating when the test stopped. Similar evolution was predicted by the crack propagation algorithm (Fig. 16b). Furthermore, the final theoretical crack length of $b_{T(th)}$=230µm was very close to the final experimental crack length of b_{exp}= 200µm.
This again confirmed the reliability of the model in predicting both $b_{ø}$ crack nucleation and crack extension: thus, for very complex stress states and variable R_K conditions.

Alternatively, the crack extension extrapolated from PD measurement was estimated around b_{PD}= 197µm, which was really close to the reference b_{exp}= 200µm provided by cross-section examination (Fig. 15b). PD strategy provided very good estimate of crack length for this loading case.

4.5 Mixed $\sigma_C(\ell_{opt})$ stress evolution: (A,B,C) sequence

This case led to experimental crack arrest in block 3 (Fig. 15c); the same behavior was predicted by the model (Fig. 15c). Examination at end of test showed a crack length of $b_{CA(exp)}$= 250µm. This result can be explained from the details of crack propagation provided by the algorithm (Fig. 16c).

The model predicted crack nucleation after 37 000 cycles, which corresponds to 54% of the first block (A). The crack propagated during the remaining loading cycle of sequence A and during the second block, B, before reaching a crack arrest condition when loading sequence C was applied. This sequential evolution can be related to the evolution of $\overline{K}^*$-z illustrated in Fig. 16c.
Fig. 16c shows how the algorithm tried to reach the third block $\overline{K}^*$ as it crossed the crack arrest condition first. This explains why a crack arrest condition appeared at the beginning of the third block. This result is consistent with the experimental evolution of V/V_0 and related b_{PD} crack length, which displayed a plateau evolution just at the beginning of the last block, C. The final predicted crack arrest length was $b_{CA(th)}$=325µm, which is 30% longer than that found on cross-section examination.

This confirms that the algorithm overestimates crack propagation. However, predicting greater crack length is a conservative approach. The lifetime algorithm seemed well adapted for predicting fretting fatigue lifetime, despite severe elastic-plastic conditions and variable loading.

This sequential evolution of the predicted crack length was compared to the experimental evolution given by the PD measurements (Fig. 15c). Crack extension extrapolated from the PD method gave a final crack length of $b_{CA(PD)}$= 170µm, which was about 30% shorter than the reference $b_{CA(exp)}$=250µm provided by cross-section examination. However, destructive test examination measures maximum projected crack length, whereas the PD method measures mean projected crack length. Mean crack length was $b_{CA(exp,mean)}$=210 µm; thus, error was reduced using the PD method, but PD crack length estimation must still be considered with caution, given the complexity of the electrical field path below the fretting interface. The predictive method, however, was calibrated on maximum crack lengths, so the differences in results may also be explained by these methodological differences.

4.6 Synthesis

The predictive algorithm provided good conservative results for all three loading sequences. It was effective in predicting both crack arrest and failure. The crack nucleation damage accumulation rule was also effective. Results could be improved by taking slip-zone wear into account [38], or by improving the elastic-plastic law: Fig. 3 clearly shows that a nonlinear rule would be more appropriate to simulate material behavior.

However, despite its simplicity, this approach appeared to be appropriate and conservative in predicting very complex fretting fatigue loading. One interesting conclusion of this analysis is that the decreasing loading stress path, as illustrated by the evolution of $\sigma_C(\ell_{opt})$ (i.e. B,A,C sequence), was the most detrimental and therefore conservative description, as was also the case for plain fatigue loading. Indeed, it was the only loading leading to failure. This result is very important because it suggests that a loading description based on crack nucleation stress is appropriate for describing fretting fatigue behavior even if it does not consider the crack extension process.

However, this conclusion needs to be confirmed by more results. Only three loading sequences, with relatively similar fretting fatigue loadings, were studied here. Cases with high fatigue stress amplitude and very low fretting amplitude were not considered and may prove to promote strong crack extension that cannot be reduced to a single $\sigma_C(\ell_{opt})$ stress variable.

5 Influence of plastic law

The preceding comparison with experimental results suggested that the proposed sequential model combining $b_{ø}$ crack nucleation and a simple description of the crack propagation stage could reliably predict fretting fatigue, even for complex loading sequences.

This requires the $\sigma_{CN(PF)}(b_{ø},N)$ crack-length endurance law, a basic Paris law, an estimated value of ΔK_{th} threshold SIF value, and an estimated value of the coefficient of friction µ. All these values can be obtained using simple plain fretting and fatigue tests.

The most “expensive“ data required by the model are the material parameters required for the cyclic elastic-plastic law (CEP). Hence, there is crucial interest in quantifying how assuming simpler material behavior, such as a monotonic elastic-plastic law (MEP) or even a simple elastic assumption (E), would impact prediction of fretting fatigue endurance.

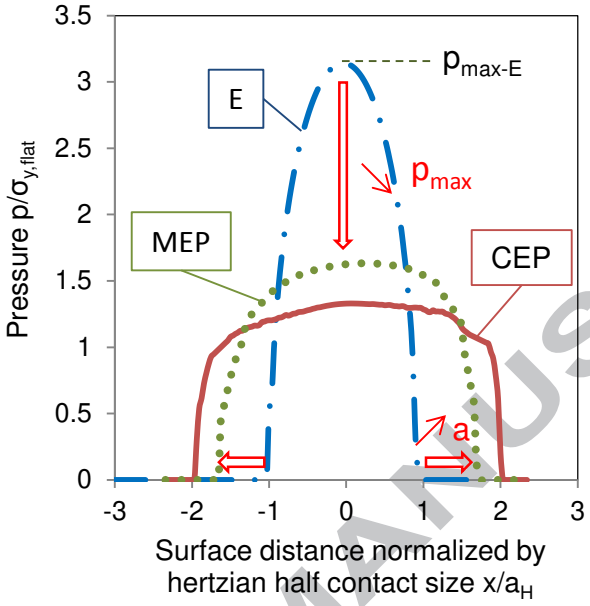

(a)

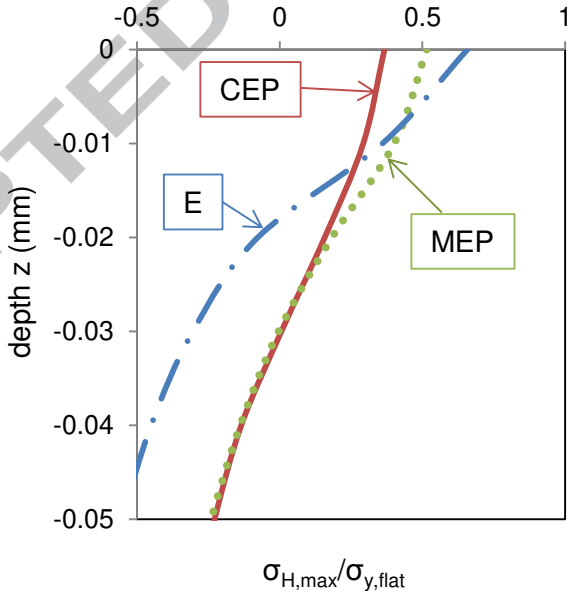

(b)

Fig. 17: Comparison with each material law hypothesis; (— · —) E, (····) MEP and (——) CEP, of (a) contact pressure profiles and (b) maximal hydrostatic stress at the contact border. Extractions on the FE simulation of (P, Q*/P=0.13, $\sigma_{F,mean}/\sigma_{y,flat}$=0.88, R_F=0.85).

Monotonic laws for both cylinder and plane were obtained from tensile tests (cf. Fig. 2a for the plane), and were implemented in FE simulations with isotropic hardening.

Compared to a fully elastic model, plasticity leads to significant plastic strain deformation in the contact region [16]. It significantly increases contact area, which tends to flatten and reduce the contact pressure profile (Fig. 17a) and consequently the maximum shear stress q_{max}, which was shown to be a controlling factor in the crack nucleation condition [39]. In accordance with the stress strain curves of Fig. 2a, the reference CEP law, previously used to establish the fretting fatigue crack model, gave more pronounced softening than the MEP law.

It is interesting to note that ℓ_{opt} was almost constant at $\ell_{opt} \approx b_{ø}/2$ whatever the material law, while b_{opt} varied slightly (Fig. 18). This variation in b_{opt} indicates that this value is to some degree dependent on the stress gradient in the contact, which softens with increasing plasticity (Fig. 17b).

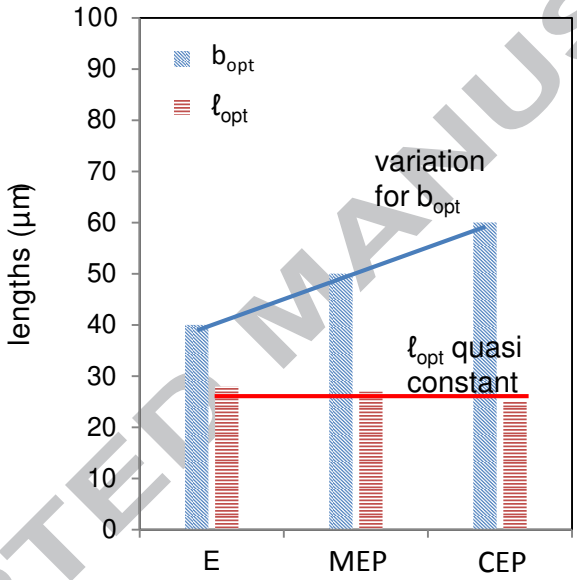

Fig. 18: ℓ_{opt} (▤) and b_{opt} (▨) evolution with material law

However, despite the strong variation in stress gradient, b_{opt} remained close to $b_{ø}$, so that it can be taken that $b_{opt}=b_{ø}$ and $\ell_{opt}=b_{ø}/2=25\mu m$, whatever the material law. Fixing these two variables, the parameters required to calibrate the model for each material behavior are shown in Table 5.

Table 5: Parameters for crack nucleation endurance Eq. 11 ($b_{ø}$, $\ell_{opt}=b_{ø}/2$)

	A_2	b_2	$\sigma_{c,inf}/\tau_d$
E	$2.5x10^4$	-0.96	0.63
MEP	$9.5x10^3$	-0.72	1
CEP	$8.5x10^3$	-0.7	1

The three variable loadings studied in section 4 were simulated again, using the E and MEP laws. Crack length results for mixed (A,B,C) and increasing loading (C,A,B) are plotted in Fig. 19a, and lifetime results for decreasing loading (B,A,C) in Fig. 19b.
The assumption of fully elastic material behavior greatly overestimated crack propagation, predicting failure in all loading cases, in contrast to the actual experimental findings: i.e., an elastic assumption provides over-conservative predictions. This was to be expected, as a

simple elastic law cannot reproduce the considerable plastic softening. Although elastic-law results were conservative, the error was too large for the description of fretting fatigue endurance to be of practical use.

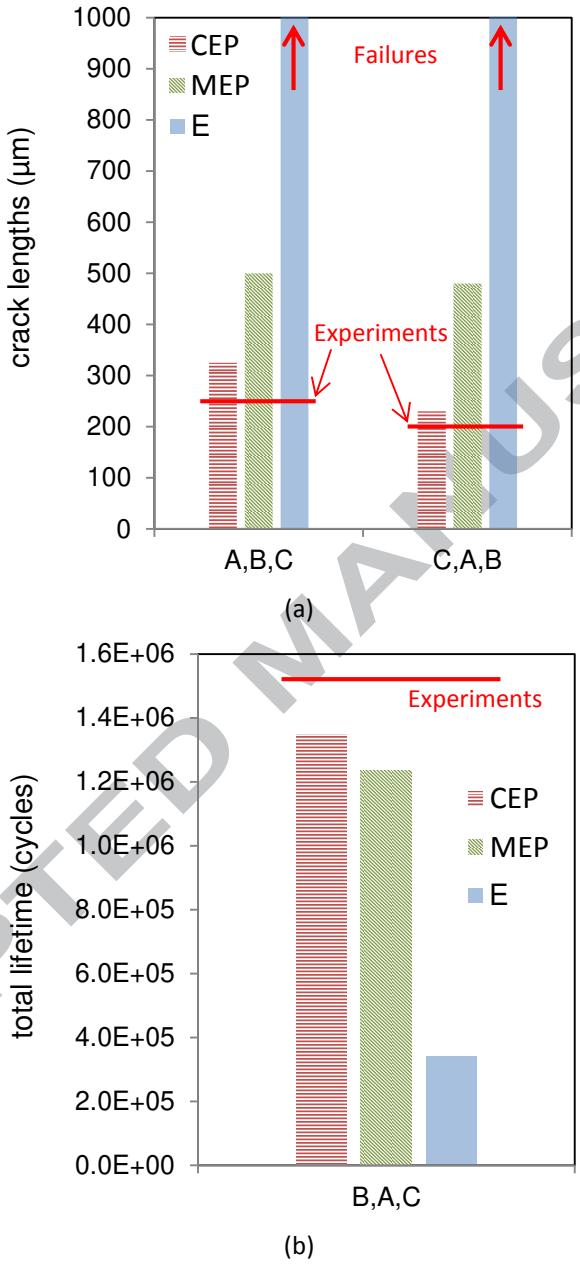

Fig. 19: (a) Predicted final crack length for case (A,B,C) and case (C,B,A) and (b) predicted lifetime for case (B,A,C) depending on the material law; simulations with following material laws ( ) E, ( ) MEP and ( ) CEP.

The cyclic law gave the best results, but error using the monotonic law was acceptable and conservative. This behavior may be explained by comparing subsurface stress profiles (Fig. 17b). Except in the first few microns below the surface, stress profiles were relatively similar. In addition, Fig. 17a shows that cyclic softening, compared to monotonic elastic-plastic law prediction, was not very great. From these results it can be concluded, while that the most accurate results are obtained using the most complete cyclic plastic law, a reasonably good estimate can be obtained using a simple monotonic law derived from simple tensile testing.

6 Conclusion

Combined experimental-modeling analysis was carried out to investigate variable fretting fatigue loading cracking prediction. Three variable loading sequences under severe plastic conditions were performed, leading to various responses. Cracking prediction was undertaken by dissociating crack nucleation life and crack propagation.

Crack nucleation was investigated using the Crossland criterion applied at a critical distance. The critical distance value was optimized to reduce prediction error: ℓ_{opt}=25µm. It was found that $\ell_{opt}=0.5b_{ø}$ with $b_{ø}$ short-to-long crack transition. This confirmed Taylor's theory, but also highlighted that this approach is satisfied if crack nucleation is defined for a b_{opt} crack nucleation length. Slight variation in b_{opt} with stress gradient was shown; but, overall, b_{opt} could be considered equal to $b_{ø}$. Crack nucleation life was estimated by coupling this criterion with the Miner linear damage accumulation law.

Crack propagation rate was investigated experimentally by using the PD method on the fatigue fretting test device. Cracking status (arrest or propagation), was monitored during tests. Crack propagation was estimated numerically using an uncoupled approach. Short crack propagation regime was omitted, as incipient crack length was $b_{opt}=b_{ø}$. The contact stress state was obtained by finite elements modeling, the mode I stress intensity factor was calculated using a weight function approach, and finally Paris law was applied on the deduced effective stress intensity range along the crack.

This approach was shown to be appropriate and conservative in predicting crack nucleation, arrest and extension for constant loading and for complex sequential fretting fatigue loading. In addition, the investigation confirmed that the decreasing $\sigma_C(\ell_{opt})$ stress path was the most detrimental and therefore conservative description, as was also the case for plain fatigue loadings, even if it does not consider the crack extension process.

This strategy was adapted to assess elastic, monotonic elastic-plastic and cyclic elastic-plastic strategies. It was demonstrated that elastic simulation systematically led to over-conservative prediction. Good predictions were achieved using simple monotonic plastic laws, despite the fact that they are not representative of the cyclic fretting fatigue loading. Only EP laws were able to reproduce the considerable softening that takes place because of plastic loading. Cyclic EP laws provided the best results, with very good prediction of crack nucleation life and crack propagation, while still maintaining safe conservative predictions. From these results it can be concluded that the most accurate results are obtained using the best material law available. However, a good first estimation can be made with monotonic laws obtained from simple tensile test.

References

[1] R.B. Waterhouse, Fretting Fatigue, Elsevier Science & Technology, 1981.

[2] D.A. Hills, D. Nowell, Mechanics of Fretting Fatigue, Wear. (1994).

[3] R.D. Mindlin, H. Deresciewicz, Elastic sphere in contact under varying oblique forces, J. Appl. Mech. 75 (1953) 327–344.

[4] K.L. Johnson, Contact Mechanics, Cambridge University press, 1985.

[5] C. Navarro, S. Muñoz, J. Domínguez, On the use of multiaxial fatigue criteria for fretting fatigue life assessment, Int. J. Fatigue. 30 (2008) 32–44.

[6] J. Vázquez, C. Navarro, J. Domínguez, A model to predict fretting fatigue life including residual stresses, Theor. Appl. Fract. Mech. 73 (2014) 144–151.

[7] R. Hojjati-Talemi, M. Abdel Wahab, J. De Pauw, P. De Baets, Prediction of fretting fatigue crack initiation and propagation lifetime for cylindrical contact configuration, Tribol. Int. 76 (2014) 73–91.

[8] F. Shen, W. Hu, Q. Meng, A damage mechanics approach to fretting fatigue life prediction with consideration of elastic–plastic damage model and wear, Tribol. Int. 82, Part A (2015) 176–190.

[9] M.P. Szolwinski, T.N. Farris, Observation, analysis and prediction of fretting fatigue in 2024-T351 aluminum alloy, Wear. 221 (1998) 24–36.

[10] S. Fouvry, P. Kapsa, L. Vincent, A multiaxial fatigue analysis of fretting contact taking into account the size effect, ASTM STP. 1367 (2000) 167–182.
[11] J.A. Araújo, D. Nowell, R.C. Vivacqua, The use of multiaxial fatigue models to predict fretting fatigue life of components subjected to different contact stress fields, Fatigue Fract. Eng. Mater. Struct. 27 (2004) 967–978.
[12] J.A. Araújo, D. Nowell, The effect of rapidly varying contact stress fields on fretting fatigue, 24 (2002) 763–775.
[13] T. Zhang, P.E. McHugh, S.B. Leen, Finite element implementation of multiaxial continuum damage mechanics for plain and fretting fatigue, Int. J. Fatigue. 44 (2012) 260–272.
[14] R. Hojjati-Talemi, M.A. Wahab, Fretting fatigue crack initiation lifetime predictor tool: Using damage mechanics approach, Tribol. Int. 60 (2013) 176–186.
[15] M.C. Baietto, E. Pierres, a. Gravouil, B. Berthel, S. Fouvry, B. Trolle, Fretting fatigue crack growth simulation based on a combined experimental and XFEM strategy, Int. J. Fatigue. 47 (2013) 31–43.
[16] C. Gandiolle, S. Fouvry, FEM modeling of crack nucleation and crack propagation fretting fatigue maps: Plasticity effect, Wear. 330-331 (2015) 136–144.
[17] J.A. Araujo, D. Nowell, Analysis of pad size effects in fretting fatigue using short crack arrest methodologies, Int. J. Fatigue. 21 (1999) 947–956.
[18] C. Gandiolle, S. Fouvry, Stability of critical distance approach to predict fretting fatigue cracking: a "ℓopt-bopt" concept, Int. J. Fatigue. 82 (2016) 199–210.
[19] C. Bosch, D. Delafosse, X. Longaygue, Effects of strain and trapping on hydrogen- induced cracking in high strength low alloy steels, Eur. Corros. Congr. 2010 (Eurocorr 2010). 2 (2010) 1558–1570.
[20] S. Fouvry, P. Kapsa, F. Sidoroff, L. Vincent, Identification of the characteristic length scale for fatigue cracking in fretting contacts, J. Phys. IV JP. 8 (1998) pp. Pr8–159–Pr8–166.
[21] J. Meriaux, S. Fouvry, K.J. Kubiak, S. Deyber, Characterization of crack nucleation in TA6V under fretting-fatigue loading using the potential drop technique, Int. J. Fatigue. 32 (2010) 1658–1668.
[22] C. Gandiolle, S. Fouvry, Experimental Analysis and Modeling of the Crack Arrest Condition Under Severe Plastic Fretting Fatigue Conditions, Procedia Eng. 66 (2013) 783–792.
[23] L. Doremus, Y. Nadot, G. Henaff, C. Mary, S. Pierret, Calibration of the potential drop method for monitoring small crack growth from surface anomalies - Crack front marking technique and finite element simulations, Int. J. Fatigue. 70 (2014) 178–185.
[24] J.M. Voisin, A.B. Vannes, L. Vincent, J. Daviot, B. Giraud, Analysis of a tube-grid oscillatory contact: methodology selection of superficial treatments, Wear. 181-183 (1995) 826–832.
[25] B. Crossland, Effect of large hydrostatic pressures on the torsional fatigue strength of an alloy steel, Proc. Int. Conf. Fatigue Met. (1956) 138–149.
[26] D. Taylor, Geometrical effects in fatigue: a unifying theoretical model, Int. J. Fatigue. 21 (1999) 413–420.
[27] R. Amargier, S. Fouvry, L. Chambon, C. Schwob, C. Poupon, Stress gradient effect on crack initiation in fretting using a multiaxial fatigue framework, Int. J. Fatigue. 32 (2010) 1904–1912.
[28] R. Ferré, S. Fouvry, B. Berthel, J. -a. Ruiz-Sabariego, Stress gradient effect on the crack nucleation process of a Ti–6Al–4V titanium alloy under fretting loading: Comparison between non-local fatigue approaches, Int. J. Fatigue. 54 (2013) 56–67.
[29] H. Kitagawa, S. Takahashi, Application of fracture mechanics to very small cracks or the cracks in the early stage, Am. Soc. Met. (1976) 627–630.
[30] M. Miner, Cumulative damage in fatigue, J. Appl. Mech. 12 (1945) 159–164.
[31] H.F. Bueckner, Weight functions and fundamental fields for the penny shaped and the half plane crack in three spaces, Int. J. Solids Struct. 23 (1987) 57–93.
[32] S. Fouvry, D. Nowell, K. Kubiak, D. a. Hills, Prediction of fretting crack propagation based on a short crack methodology, Eng. Fract. Mech. 75 (2008) 1605–1622.
[33] A. De Pannemaecker, S. Fouvry, J.Y. Buffiere, Introduction of a reverse simulation approach to identify the fatigue stress intensity factor crack arrest threshold from fretting cracking experiments, Tribol. Int. 76 (2014) 122–132.
[34] A. de Pannemaecker, S. Fouvry, M. Brochu, J.Y. Buffiere, Identification of the fatigue stress intensity factor threshold for different load ratios R: From fretting fatigue to C(T) fatigue experiments, Int. J. Fatigue. 82 (2016) 211–225.
[35] C. Vallellano, J. Domínguez, a. Navarro, Influence of R ratio and stick zone eccentricity on the prediction of the fretting fatigue limit with spherical contact, Int. J. Fatigue. 29 (2007) 1208–1219.
[36] D. Kujawski, A fatigue crack driving force parameter with load ratio effects, Int. J. Fatigue. 23 (2001) 239–246.
[37] M. El Haddad, K. Smith, T. Topper, Fatigue crack propagation of short cracks, J Engng Mater Technol. 101 (1979) 6.
[38] J. Madge, S. Leen, P. Shipway, A combined wear and crack nucleation–propagation methodology for fretting fatigue prediction, Int. J. Fatigue. 30 (2008) 1509–1528.
[39] S. Fouvry, H. Gallien, B. Berthel, From uni- to multi-axial fretting-fatigue crack nucleation: Development of a stress-gradient-dependent critical distance approach, Int. J. Fatigue. 62 (2014) 194–209.